



# Diagnosing the transition layer at extratropical latitudes using MLS O<sub>3</sub> and MOPITT CO analyses

J. Barré<sup>1,\*</sup>, L. El Amraoui<sup>1</sup>, P. Ricaud<sup>1</sup>, W. A. Lahoz<sup>1,3</sup>, J.-L. Attié<sup>1,2</sup>, V.-H. Peuch<sup>4</sup>, B. Josse<sup>1</sup>, and V. Marécal<sup>1</sup>

<sup>1</sup>CNRM-GAME, Météo-France and CNRS URA 1357, Toulouse, France

<sup>2</sup>Laboratoire d'Aérodynamique, Université de Toulouse, CNRS/INSU, Toulouse, France

<sup>3</sup>Norsk Institutt for Luftforskning, 2027 Kjeller, Norway

<sup>4</sup>European Centre for Medium-Range Weather Forecasts, Shinfield Park, Reading, UK

\* now at: National Center for Atmospheric Research, Boulder, Colorado, USA

Correspondence to: J. Barré (barre.jerome@yahoo.fr)

Received: 28 June 2012 – Published in Atmos. Chem. Phys. Discuss.: 28 August 2012

Revised: 10 June 2013 – Accepted: 27 June 2013 – Published: 30 July 2013

**Abstract.** The behavior of the extratropical transition layer (ExTL) is investigated using a chemistry transport model (CTM) and analyses derived from assimilation of MLS (Microwave Limb Sounder) O<sub>3</sub> and MOPITT (Measurements Of Pollution In The Troposphere) CO data. We firstly focus on a stratosphere–troposphere exchange (STE) case study that occurred on 15 August 2007 over the British Isles (50° N, 10° W). We evaluate the effect of data assimilation on the O<sub>3</sub>–CO correlations. It is shown that data assimilation disrupts the relationship in the transition region. When MLS O<sub>3</sub> is assimilated, CO and O<sub>3</sub> values are not consistent between each other, leading to unphysical correlations at the STE location. When MLS O<sub>3</sub> and MOPITT CO assimilated fields are taken into account in the diagnostics the relationship happens to be more physical. We then use O<sub>3</sub>–CO correlations to quantify the effect of data assimilation on the height and depth of the ExTL. When the free-model run O<sub>3</sub> and CO fields are used in the diagnostics, the ExTL distribution is found 1.1 km above the thermal tropopause and is 2.6 km wide (2 $\sigma$ ). MOPITT CO analyses only slightly sharpen (by –0.02 km) and lower (by –0.2 km) the ExTL distribution. MLS O<sub>3</sub> analyses provide an expansion (by +0.9 km) of the ExTL distribution, suggesting a more intense O<sub>3</sub> mixing. However, the MLS O<sub>3</sub> analyses ExTL distribution shows a maximum close to the thermal tropopause and a mean location closer to the thermal tropopause (+0.45 km). When MLS O<sub>3</sub> and MOPITT CO analyses are used together, the ExTL shows a mean location that is the closest to the thermal tropopause (+0.16 km). We also extend the study at the

global scale on 15 August 2007 and for the month of August 2007. MOPITT CO analyses still show a narrower chemical transition between stratosphere and troposphere than the free-model run. MLS O<sub>3</sub> analyses move the ExTL toward the troposphere and broaden it. When MLS O<sub>3</sub> analyses and MOPITT CO analyses are used together, the ExTL matches the thermal tropopause poleward of 50°.

## 1 Introduction

The upper troposphere/lower stratosphere (UTLS) plays a key role in chemistry–climate interactions. Carbon monoxide (CO) and ozone (O<sub>3</sub>) concentrations change rapidly across the UTLS. High concentrations of O<sub>3</sub> (low concentrations of CO) in the lower stratosphere contrast with low concentrations of O<sub>3</sub> (high concentrations of CO) in the upper troposphere. Holton et al. (1995) defined the lowermost stratosphere (LMS) as being below the 380 K isentrope and above the dynamical tropopause (usually defined in a range between 1.5 and 3.5 potential vorticity units (PVU)). Previous studies, using in situ measurements of stratospheric and tropospheric trace gases, have shown that the LMS has intermediate characteristics between the troposphere and the stratosphere (Fischer et al., 2000; Hoor et al., 2002; Pan et al., 2004). Rapid changes in time and space of tracers at the UTLS are controlled by mixing processes between the stratosphere and the troposphere. An extratropical transition layer (ExTL) of atmospheric tracers is present in the LMS above

the extratropical dynamical tropopause. The World Meteorological Organization (2003) defined the ExTL as a transition layer with chemical characteristics intermediate between the upper troposphere and the lower stratosphere maintained by exchanges across the tropopause.

Diagnostics using tracer–tracer correlation can locate the ExTL in an empirical way. Fischer et al. (2000), Hoor et al. (2002) and Pan et al. (2004) used aircraft in situ measurements to provide an analysis of trace gas ( $\text{H}_2\text{O}$ , CO,  $\text{CO}_2$ ,  $\text{N}_2\text{O}$ ,  $\text{NO}_y$  and  $\text{O}_3$ ) correlations in the LMS. Trace gas correlations have been shown to be an effective method to diagnose stratosphere–troposphere exchange (STE) and mixing processes in the LMS. Tracer–tracer correlation methods in the LMS are introduced by Fischer et al. (2000). A following study, Hoor et al. (2002), attempted to diagnose the seasonal variation of the tracer–tracer relationship in the LMS. These two studies have concluded that a transition layer is formed in the LMS as a result of troposphere-to-stratosphere transport. Pan et al. (2004) introduced the use of tropopause-relative coordinates in addition of the tracer–tracer correlation methods, and Pan et al. (2007) proposed a set of three diagnostics to evaluate the representation of chemical transport processes in the extratropical tropopause.

This study uses the diagnostics proposed by Pan et al. (2007) that define a statistical way to characterize the location and the thickness of the mixing layer using tracer–tracer relationships. Diagnosing ExTL height and thickness from tracer–tracer relationships is empirical but remains a powerful tool for characterizing the extratropical UTLS region. These types of diagnostics rely on a statistical characterization of the transition layer instead of attempting to identify the tropopause as a single point. Results from these diagnostics therefore provide new perspectives on the transition from stratosphere to troposphere. Hegglin et al. (2009) showed that these diagnostics can be applied to satellite measurements of  $\text{O}_3$ , CO and  $\text{H}_2\text{O}$  to characterize the ExTL seasonal and latitudinal variations in height and depth at the global scale. A multi-model assessment showed that models with coarse vertical resolution are unable to represent faithfully the ExTL at extratropical latitudes (Hegglin et al., 2010). Due to their coarse resolution, models overestimate the spread and the location in height of the ExTL.

Data assimilation, which combines observational information and a priori information from a model in an objective way (Kalnay, 2003), has the capability to combine satellite trace gas measurements and chemistry transport models. Data assimilation studies that focused on UTLS chemical fields started with Cathala et al. (2003), who assimilated subsonic flight-level observations of ozone. Later, Semane et al. (2007) assimilated  $\text{O}_3$  data from a limb sounder (Michelson Interferometer for Passive Atmospheric Sounding) to diagnose a case study of STE over arctic regions. It has been shown that assimilation of stratospheric ozone data from a limb sounder improves the spatial struc-

ture of the ozone fields in the UTLS. Jackson (2007) and Stajner et al. (2008) have assimilated MLS (Microwave Limb Sounder)  $\text{O}_3$  data and shown the added value of data assimilation on UTLS ozone fields in the tropics and in the extratropics. Wargan et al. (2010) use the Ozone Monitoring Instrument and MLS  $\text{O}_3$  in a data assimilation experiment to discuss the improvements of data assimilation in the spatial ozone structure in the UTLS and the related limitations due to the model resolution. Barré et al. (2012) have assimilated MLS  $\text{O}_3$  at low and high horizontal resolution, and show the impact of data assimilation and resolution on the UTLS spatial structure and on the tropospheric ozone fields. Barret et al. (2008) assimilated MLS CO data to investigate the transport pathway of CO in the African upper troposphere during the monsoon season. Finally, El Amraoui et al. (2010) have used MLS  $\text{O}_3$  and MOPITT (Measurement Of Pollution In The Troposphere) CO to diagnose a STE event. This last study showed that assimilated MOPITT CO allows for a better qualitative description of the stratospheric intrusion event.

To constrain the model used in this study, we assimilate  $\text{O}_3$  stratospheric profiles from Aura/MLS and Terra/MOPITT CO tropospheric profiles into the MOCAGE (Modèle de Chimie Atmosphérique à Grande Echelle) chemical transport model (CTM). Data assimilation has the capability to overcome possible deficiencies of the MOCAGE model in the UTLS (see, e.g., Semane et al., 2007; Barret et al., 2008; El Amraoui et al., 2010; Barré et al., 2012). The aim of this study is to quantify the impact of the assimilation of  $\text{O}_3$  and CO data on the UTLS at extratropical latitudes. We use the same case study as presented by El Amraoui et al. (2010) that considers a deep stratospheric intrusion on 15 August 2007 over the British Isles ( $50^\circ\text{N}$ ,  $10^\circ\text{W}$ ). In this previous study, detailed validation demonstrated the capability of CO and  $\text{O}_3$  analyses to better represent the STE. The set of diagnostics proposed by Pan et al. (2007) are used here to quantify the capability of CO and  $\text{O}_3$  analyses to represent the STE event. We also propose to extend the set of diagnostics from regional to global scales in the extratropics for the month of August 2007. This allows for us to quantify the capability of MOPITT CO and MLS  $\text{O}_3$  assimilated fields to better estimate the chemical ExTL behavior, from a single STE event at the regional scale to an average state of the atmosphere at the global scale. To our knowledge, this is the first time that these diagnostics have been used on chemical analyses from different types of satellite measurements (nadir and limb).

The paper is structured as follows. Section 2 provides the description of the model, the remotely sensed data and the assimilation system. Section 3 provides a brief description of the STE event in August 2007 that was fully evaluated by El Amraoui et al. (2010). A set of diagnostics proposed by Pan et al. (2007) are used on this case study for the different assimilation experiments. Section 4 extends these diagnostics to the global scale in the extratropics in August 2007. Section 5 provides a discussion of results and conclusions.

## 2 Methodology

### 2.1 CTM and data assimilation system

The MOCAGE model is a three-dimensional CTM for the troposphere and the stratosphere (Peuch et al., 1999) that simulates the interactions between physical and chemical processes. It uses a semi-Lagrangian advection scheme (Josse et al., 2004) to transport the chemical species. It has 47 hybrid levels from the surface to  $\sim 5$  hPa with a resolution of about 150 m in the lower troposphere increasing to 800 m in the upper troposphere, and then constant in the stratosphere. Turbulent diffusion is calculated with the scheme of Louis (1979), and convective processes with the scheme of Bechtold et al. (2001). The chemical scheme used in this study is RACMOBUS. It is a combination of the stratospheric scheme REPROBUS (Reactive Processes Ruling the Ozone Budget in the Stratosphere, Lefèvre et al., 1994) and the tropospheric scheme RACM (Regional Atmospheric Chemistry Mechanism, Stockwell et al., 1997). It includes 119 individual species with 89 prognostic variables and 372 chemical reactions. MOCAGE has the flexibility to be used for stratospheric (El Amraoui et al., 2008a), tropospheric (Dufour et al., 2005) and UTLS studies (Ricaud et al., 2007; Barré et al., 2012). The meteorological analyses of Météo-France, ARPEGE (Courtier et al., 1991), are used to provide meteorological fields. In this study, the model has a global domain with an horizontal resolution of  $2^\circ \times 2^\circ$ .

The assimilation system used in this study is MOCAGE-PALM (Massart et al., 2005), implemented within the PALM framework (Buis et al., 2006). The technique used is 3-D-FGAT (first guess at appropriate time, Fisher and Anderson (2001)). This technique is a compromise between the 3-D-Var (3-D-variational) and the 4-D-Var (4-D-variational) methods. It compares the observations and the model background taking into account the measurement time, and assumes that the increment to be added to the background state is constant over the entire assimilation window (in this case 3 h). The choice of this technique limits the size of the assimilation window, since it has to be short enough compared to chemistry and transport timescales. It has been validated during the assimilation of ENVISAT data project (ASSET, Lahoz et al. (2007)), and has produced good quality results compared to independent data and other assimilation systems (Geer et al., 2006). MOCAGE-PALM has been used to assess the quality of satellite  $O_3$  measurements (Massart et al., 2007). The MOCAGE-PALM, assimilation products have been used in many atmospheric studies in relation to the  $O_3$  loss in the Arctic vortex (El Amraoui et al., 2008a), tropics–midlatitudes exchange (Bencherif et al., 2007), STE (Semane et al., 2007), exchange between the polar vortex and the midlatitudes (El Amraoui et al., 2008b) and diagnosing STE from  $O_3$  and CO fields (El Amraoui et al., 2010).

### 2.2 Aura/MLS $O_3$ and Terra/MOPITT CO observations

The MLS instrument onboard Aura uses limb sounding to measure chemical constituents (such as  $O_3$ ) and dynamical tracers between the upper troposphere and the lower mesosphere (Waters et al., 2006). It provides global coverage with about 3500 profiles per day between  $82^\circ$  N and  $82^\circ$  S. In this study, we use version 2.2 of the MLS  $O_3$  dataset. This version provides profiles with about 3–5 km vertical resolution between 215 and 0.46 hPa. The along-track resolution of  $O_3$  is  $\sim 200$  km between 215 and 10 hPa. The MLS data are selected following quality flags recommended in the MLS description document (see [http://mls.jpl.nasa.gov/data/v2\\_data\\_quality\\_document.pdf](http://mls.jpl.nasa.gov/data/v2_data_quality_document.pdf)). Measurements above 10 hPa are not used because of the upper limit of the MOCAGE model, 5 hPa. The measurement precision is in 0.04 ppmv (parts per million by volume) for lower altitudes (215 hPa) and of 0.2 ppmv for higher altitudes (10 hPa).

The MOPITT instrument (Drummond and Mand, 1996) is onboard the Terra platform and measures tropospheric CO with nadir sounding. The horizontal resolution of MOPITT CO data (version 3) is  $22 \text{ km} \times 22 \text{ km}$ . To prepare the MOPITT data for assimilation, super-observations are done by averaging data in latitude–longitude bins of  $2^\circ \times 2^\circ$ . The super-observations give around 8000 daily vertical profiles that are retrieved on seven pressure levels (surface, 850, 700, 500, 350, 250 and 150 hPa). Information on the vertical sensitivity is provided by the averaging kernels, which are also averaged and are taken into account in the assimilation system. At 500 hPa, the retrieval uncertainties are approximately 20 % in the tropics and at midlatitudes, and 30–40 % at high latitudes.

### 2.3 Assimilation experiments

In this study, we use the same assimilation experiments performed by El Amraoui et al. (2010), hereafter LEA2010. The initial conditions for the assimilation were obtained by a free-model run started from the April climatological field. The assimilation of MLS  $O_3$  stratospheric and UTLS profiles and the assimilation of MOPITT CO tropospheric profiles started on 20 July 2007 and involve two independent runs (i.e., the assimilation experiments of  $O_3$  and CO are done separately). We estimate this spin-up period to be sufficient enough to have both  $O_3$  and CO fields well balanced with respect to the atmospheric chemistry and dynamics. The assimilated fields of  $O_3$  and CO have been validated for the month of July and August 2007 by LEA2010 using measurements from ozone sondes, aircraft and other remote sensing instruments. This validation exercise showed better agreement of the analyses of each chemical species than the free-model runs.

$O_3$  assimilated fields have been evaluated using different types of independent measurements. The bias, root-mean-square error (RMS) and correlation between modeled  $O_3$  and

aircraft measurements are  $-33$  ppbv,  $38.5$  ppbv and  $0.83$ , respectively. The bias, RMS and correlation between assimilated  $O_3$  and aircraft measurements  $11.5$  ppbv,  $22.4$  ppbv and  $0.93$ , respectively. The correlation coefficients are  $0.66$  and  $0.82$  between OMI total columns (Ozone Monitoring Instrument) and the free-model run and between OMI total columns and the assimilated MLS field, respectively. In a further comparison using an ozonesonde, it is shown that the model underestimates the  $O_3$  concentrations, particularly between  $300$  and  $150$  hPa. The assimilation of MLS  $O_3$  profiles corrects this underestimation since the agreement between ozonesonde measurements and the MLS assimilated profile is better than the free-model run profile (see Fig. 7 in LEA2010).

As for  $O_3$ , CO fields have also been evaluated using different types of independent measurements. The bias, RMS and correlation between modeled CO and aircraft measurements are  $-6.3$  ppbv,  $16.6$  ppbv and  $0.71$ , respectively. The bias, RMS and correlation between assimilated CO and aircraft measurements are  $3.16$  ppbv,  $13$  ppbv and  $0.79$ , respectively. AIRS (Atmospheric Infrared Sounder) total CO columns are also used for evaluation. The correlation coefficients between AIRS and modeled CO and between AIRS and assimilated MOPITT CO are  $0.51$  and  $0.75$ , respectively.

### 3 STE case study on 15 August 2007

In this section, we present the case study of a STE event on 15 August 2007 over the British Isles. Figure 1 shows the  $O_3$  and CO fields for MOCAGE and MOCAGE-PALM (MLS  $O_3$  analyses and MOPITT CO analyses) in the UTLS (260 hPa) between  $35^{\circ}$ – $75^{\circ}$  N and  $35^{\circ}$  W– $25^{\circ}$  E. Figure 2 shows longitude–pressure cross sections at  $59^{\circ}$  N between  $35^{\circ}$  W and  $25^{\circ}$  E. These figures display the free-model run CO fields (hereafter model CO) and MOPITT CO analyses (hereafter CO analyses) and free-model run  $O_3$  fields (hereafter model  $O_3$ ) and MLS  $O_3$  analyses (hereafter  $O_3$  analyses). The  $380$  K isentrope (black solid line) and the  $2$  PVU (white solid line) contours define the LMS height range. The STE event shows a deep stratospheric intrusion with high  $O_3$  values (low CO values) coming from polar latitudes spreading southward over western Europe.

In the latitude–longitude maps,  $O_3$  analyses (Fig. 1c) show increased values in the STE structure compared to the model. Conversely, CO analyses (Fig. 1d) tend to exhibit decreased values in the STE structure compared to the model and also increased values around the STE. Along the vertical,  $O_3$  analyses (Fig. 2c) show increased  $O_3$  in the  $200$ – $300$  hPa layer compared to the model  $O_3$  field. For CO analyses, a minimum of CO in the cross section (Fig. 2d) is in good agreement with the stratospheric intrusion (between  $10$  and  $0^{\circ}$  W) down to  $400$  hPa. At the LMS height range and at longitudes around the intrusion, the CO assimilated fields also display higher values than the model CO fields. LEA2010 also

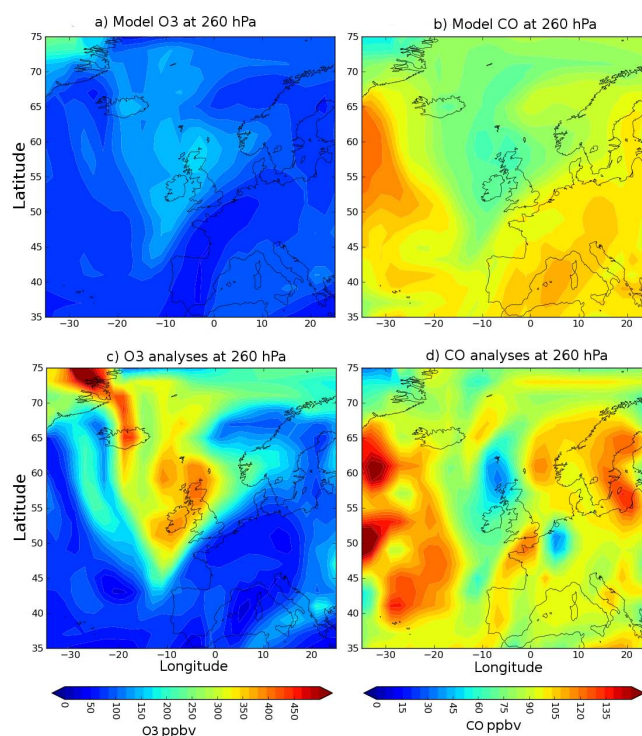


**Fig. 1.** Longitude–latitude maps at 260 hPa of model  $O_3$  (a), model CO (b),  $O_3$  analyses (c) and CO analyses (d) for 15 August 2007 at 12:00 UTC.

showed that CO analyses and  $O_3$  analyses are in better agreement with independent data (MOZAIC flights, WOUDC ozone sondes and remotely sensed data) than the free-model run. A perspective of LEA2010 was to focus on the quantification of the contribution of  $O_3$  and CO assimilated species in the chemical mixing process between the stratosphere and the troposphere. In a CTM context, none of the meteorological fields are modified and only the chemical fields are modified, through the assimilation process. The ExTL diagnosed in this study is then the layer characterizing the chemical transition. In this study, we diagnose how this chemical transition, i.e., an estimate of the ExTL, is modified through the different assimilation experiments. By modifying only the chemical fields, the air mass mixing itself is not modified by the assimilation, but the diagnosed mixing process using the chemical tracer–tracer relationship is. When we refer to mixing in the text it is about diagnosed mixing using the chemical fields. To quantify the contribution of each experiment presented here, we have used the three diagnostics discussed by Pan et al. (2007):

1.  $O_3$ –CO correlations: to empirically select the CO and  $O_3$  values that belong to the stratosphere, the troposphere and the ExTL.
2. Profile comparisons using relative altitude coordinates: to remove the geophysical variability from the planetary

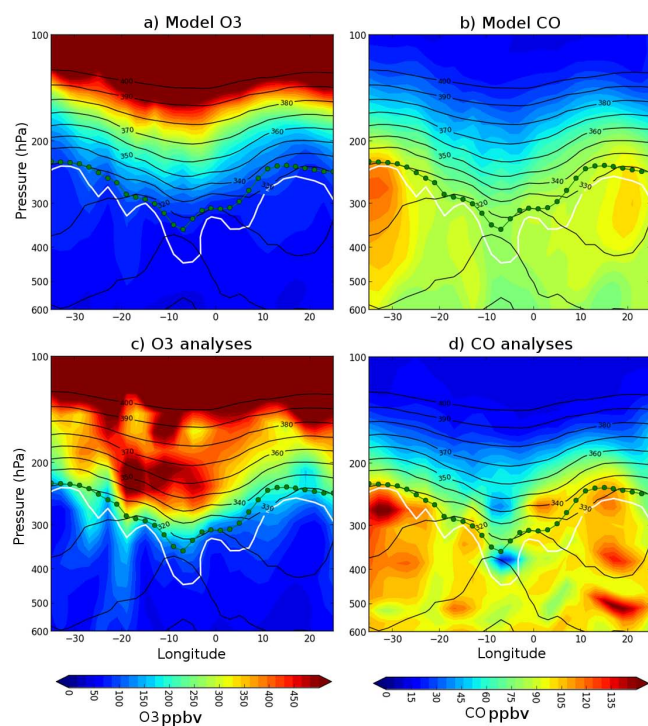


**Fig. 2.** Zonal cross sections at 59° N between 40° W and 40° E longitude and between 600 and 100 hPa in the vertical for model O<sub>3</sub> (a), model CO (b), O<sub>3</sub> analyses (c) and CO analyses (d). The white line corresponds to the 2 PVU contour. The black lines correspond to the 300 to 400 K isentropic contours by 10 K intervals. The line with green circles corresponds to the thermal tropopause. Panels are for 15 August 2007 at 12:00 UTC.

wave activity and to diagnose the effect of data assimilation on the UTLS CO and O<sub>3</sub> gradients.

3. Sharpness of the transition: to quantify the depth and the location of the ExTL.

### 3.1 Diagnostic 1: O<sub>3</sub>–CO correlations

Tracer–tracer correlation methods help to identify the chemical transition between the stratosphere and the troposphere and the mixing processes in the LMS (Fischer et al., 2000; Zahn et al., 2000; Hoor et al., 2002, 2004; Pan et al., 2004, 2007). Tracer–tracer correlation methods are effective to diagnose mixing in the ExTL. These methods follow an empirical process to select the tropospheric values, transition layer values and stratospheric values. It is also important to know that the diagnostic would give different results if different tracers are used, for example O<sub>3</sub>–H<sub>2</sub>O correlations (Heglin et al., 2009). In this section, we use O<sub>3</sub>–CO correlations to determine empirically the chemical transition layer from model and analyzed fields. Diagnosing the chemical transition layer using O<sub>3</sub>–H<sub>2</sub>O is out of the scope of this paper since H<sub>2</sub>O has not been assimilated. Figure 3 shows the O<sub>3</sub>–

CO relationships for model O<sub>3</sub> vs. model CO (Fig. 3a), O<sub>3</sub> analyses vs. model CO (Fig. 3b), model O<sub>3</sub> vs. CO analyses (Fig. 3c) and O<sub>3</sub> analyses vs. CO analyses (Fig. 3d). As described by Pan et al. (2007), the O<sub>3</sub>–CO relationship is “L” shaped and has a stratospheric branch (high O<sub>3</sub> values and low CO values) and a tropospheric branch (low O<sub>3</sub> values and high CO values). These two branches can be represented by an approximate quasi-linear relation between O<sub>3</sub> and CO. Between these two branches the relationship between O<sub>3</sub> and CO is nonlinear due to the different chemical composition of the stratosphere and the troposphere.

We have applied the O<sub>3</sub>–CO correlation diagnostic on 15 August 2007 12:00 UTC between 30° W–10° E and 40–65° N where the STE takes place. We have also applied the diagnostics in the 700–80 hPa vertical range to avoid the boundary layer values and the high stratospheric ozone values. The stratospheric branch, where high O<sub>3</sub> variability and low CO variability are observed, is empirically identified with a selection criterion defined by Pan et al. (2007). In Fig. 2, low CO values are mainly located in the stratosphere (above the 380 K isentrope) in the MOCAGE CO and in the MOPITT CO analyses. A quadratic fit is done with the CO values less than 25 ppbv. CO values that are below +3 $\sigma$  (where  $\sigma$  is the standard deviation of the selected data) from the fit are considered as stratospheric (blue dots in Fig. 3). The tropospheric branch, where low O<sub>3</sub> variability and high CO variability are observed, is also empirically identified with a selection criterion defined by Pan et al. (2007). In Fig. 2, these low O<sub>3</sub> values are mainly located in the troposphere (below the 2 PVU line) in the MOCAGE O<sub>3</sub> and in the MLS O<sub>3</sub> analyses. A linear fit is done with O<sub>3</sub> values lower than 70 ppbv. O<sub>3</sub> values that are lower than +3 $\sigma$  from the fit are considered as tropospheric (red dots in Fig. 3). Between these two branches a set of points (green dots in Fig. 3) mark a chemical transition between the stratosphere and the troposphere.

The “L” shape is detected in the four O<sub>3</sub>–CO correlations, but the transition differs significantly between them. The transition is composed by mixing lines corresponding to O<sub>3</sub>–CO vertical relationships for each latitude–longitude location of the model. To illustrate this concept we have plotted in black the points located between 20 and 0° W on the 59° N vertical plane corresponding to the stratospheric air mass intrusion displayed in the cross sections (Fig. 2). We also have overplotted a quadratic fit of these points in Fig. 3; coefficients of the fit are provided in Table 1. The model O<sub>3</sub> vs. model CO shows a “convex” and compact relationship in the chemical transition. This “convex” behavior can be understood as a transition of a chemical regime between the stratosphere and the troposphere. Hoor et al. (2002) explains the convex curvature of the correlation as the result of a combination of dynamical and photochemical effects. However, in Hoor et al. (2002), the convex curvature in the correlation was observed during late winter (March), whereas a linear relationship is observed in summer (July). A linearity in the

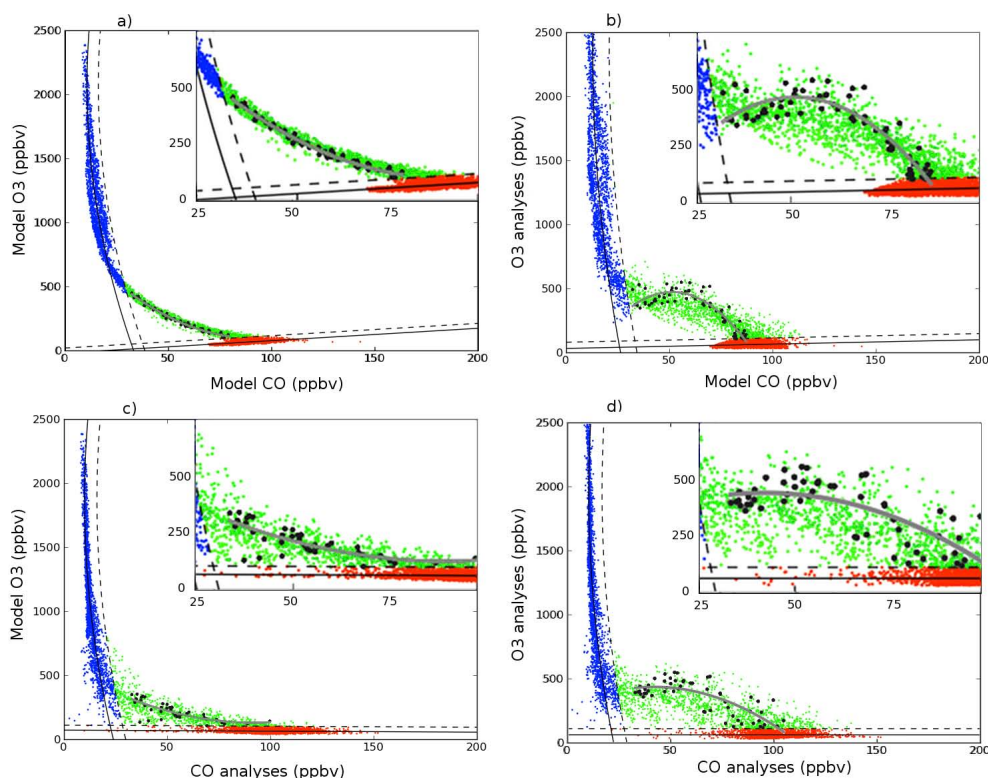


**Fig. 3.** Comparisons of the O<sub>3</sub>–CO relationships between model O<sub>3</sub> vs. model CO (a), O<sub>3</sub> analyses vs. model CO (b), model O<sub>3</sub> vs. CO analyses (c) and O<sub>3</sub> analyses vs. CO analyses (d) in the area between 30° W–10° E and 40–65° N on 15 August 2007 at 12:00 UTC. In all cases, red and blue dots are identified as tropospheric and stratospheric model grid points, respectively. Black solid lines indicate fits to tropospheric and stratospheric values and the dashed lines are the +3σ values (where σ is the standard deviation of the selected data) from those fits. The green dots are identified as the transition between stratospheric and tropospheric air. The transitional points between 20 and 0° W on the 59° N vertical plane are in black and are fitted by the gray line (see text for details). Within each plot box a zoom of the transition layer is provided (top right) on each panel.

transition indicates a rapid mixing of tropospheric and stratospheric air masses. In our case study, the convex curvature diagnosed in the O<sub>3</sub>–CO correlations does not indicate a rapid mixing process as expected in a STE.

Following Plumb (2007) the compactness of the tracer–tracer correlation is proportional to the variation of the chemical fields along isentropic surfaces. In the case of the free-model run and in the region of interest, the chemical variability at tropopause altitudes is relatively low following the isentropic lines (see Fig. 2a and b). This low variability is diagnosed by a compact correlation between O<sub>3</sub> and CO values in the transition layer. The dots located in the transition region are merged in the same slope, indicating the same behavior of the O<sub>3</sub>–CO correlations at different locations. Hoor et al. (2002) also suggests that mixing occurring only episodically, or involving very different tropospheric air masses (e.g., rather different CO concentrations), would spread the compact relationship in the transition layer. Then the low spread in the O<sub>3</sub>–CO correlations observed here suggests a low mixing activity represented by the model during the STE.

Compared to the model O<sub>3</sub> vs. model CO correlations, the O<sub>3</sub> analyses vs. model CO correlations show an increase of O<sub>3</sub> values in the chemical transition. The relationship between O<sub>3</sub> analyses and model CO (Fig. 3b) is less compact, showing different shapes of mixing lines at different locations. This illustrates the O<sub>3</sub> variability following the isentropes induced by MLS assimilation at tropopause altitudes (see Fig. 2c). As mentioned above, a less compact O<sub>3</sub>–CO relationship corresponds to a mixing process occurring episodically. Some of the mixing lines show a strong “concave” shape owing to the stratospheric air mass intruding the troposphere, characterized by high ozone mixing ratio values. In Fig. 2c, a maximum of ozone is observed between 200 and 250 hPa and between 20 and 0° W corresponding to stratospheric air masses intruding the upper troposphere. However, the free-model CO fields do not show a strong CO decrease in the location of the intrusion. The CO and O<sub>3</sub> values are not consistent between each other, leading to a specific “concave” correlation at the location of the intrusion. In other locations, the O<sub>3</sub>–CO relationship does not show a concave correlation.

**Table 1.** Fitting coefficients for the ExTL of O<sub>3</sub>–CO correlations, assuming a quadratic form  $y = a_2x^2 + a_1x + a_0$ . CO and O<sub>3</sub> values are defined by  $x$  and  $y$ , respectively.

	$a_2$	$a_1$	$a_0$
model O <sub>3</sub> vs. model CO	$9.73 \times 10^{-2}$	$-1.78 \times 10^1$	$9.11 \times 10^2$
O <sub>3</sub> analyses vs. model CO	$-2.99 \times 10^{-1}$	$3.07 \times 10^1$	$-3.17 \times 10^2$
model O <sub>3</sub> vs. CO analyses	$5.31 \times 10^{-2}$	$-9.75$	$5.77 \times 10^2$
O <sub>3</sub> analyses vs. CO analyses	$-8.84 \times 10^{-2}$	$7.39$	$2.80 \times 10^2$

The model O<sub>3</sub> vs. CO analyses correlations (Fig. 3c) show a more angular “L” shape and a less compact relationship than model O<sub>3</sub> vs. model CO correlations. The assimilation process induces a less compact relationship that is due to the increased variability of the upper tropospheric CO values. As mentioned above, this suggests more diagnosed mixing between the stratosphere and the troposphere. In the MOPITT analyses, the CO values are more variable following the isentropes. In this case CO values are decreased in the chemical transition and tend to be increased in the upper troposphere except in the location of the intrusion where CO values are decreased (see Fig. 2d). In general, mixing lines tend to be pulled toward the lower-left corner, corresponding to less mixing. At the location of the intrusion, the relationship is the less curved, and the slope of the fit is decreased compared to the model O<sub>3</sub> vs. model CO fit (see Table 1).

In this comparison (i.e., model O<sub>3</sub> vs. CO analyses), only CO fields are assimilated, and O<sub>3</sub> fields are not. As diagnosed for O<sub>3</sub> analyses vs. model CO correlations, the CO analyzed fields are then not chemically consistent with model O<sub>3</sub> fields. However, correlation plots do not show a specific “concave” curve fit because a tropospheric CO product (MOPITT CO) is assimilated. Even if CO is decreased in the location of the intrusion and increased around it (Fig. 2d), the dots in the correlation plot will only move in the CO dimension. The MOPITT sensitivity is mainly tropospheric, and detects the intrusion as a minimum of CO visible in the analyses between 300 and 400 hPa and between 20 and 0° W (Fig. 2d) (where the dynamical tropopause is the lowest in height). Unlike the O<sub>3</sub> analyzed fields, no drastic changes can be noted in the CO analyzed fields in the lower stratosphere (around 360 K and 380 K levels). For this reasons, MOPITT CO analyses do not modify significantly the curvature of the mixing lines.

The O<sub>3</sub> analyses vs. CO analyses correlations show both the effect of MLS O<sub>3</sub> analyses and MOPITT CO analyses. In the chemical transition, O<sub>3</sub> values are increased whereas CO values are decreased. The spread of the O<sub>3</sub>–CO correlations in the chemical transition is increased compared to the other O<sub>3</sub>–CO correlations, showing an increased spatial variability of the O<sub>3</sub>–CO mixing lines. At the location of the intrusion the mixing lines still show a concave shape but with a slight curvature compared to the O<sub>3</sub> analyses vs. model CO mixing lines (see Table 1). This is due to a better O<sub>3</sub>–CO consis-

tency when both species are assimilated than when only one is assimilated. In this section, we use O<sub>3</sub>–CO correlations to select empirically the chemical transition points in order to have an estimate of the ExTL. The impact of assimilation of O<sub>3</sub> and CO fields on the correlations is discussed. We also diagnose in the next sections how the assimilation of MOPITT CO and MLS O<sub>3</sub> data affects the spatial extent of the estimated ExTL.

### 3.2 Diagnostic 2: profile comparisons using relative altitude coordinates

In the second diagnostic, we analyze the tracer behavior in altitude coordinates relative to a chosen tropopause level. Because rapid changes in height of tracer concentrations happen near the tropopause, it is helpful to use a tropopause-relative vertical coordinate to reduce the geophysical variability caused by wave activity at synoptic and planetary scales. The thermal tropopause has been used as a reference level by Pan et al. (2007) and Pan et al. (2004) to calculate relative altitudes. The thermal tropopause and the dynamical tropopause can provide double thermal or dynamical tropopause features related to Rossby-wave breaking processes and associated transport (Pan et al., 2009; Homeyer et al., 2010). These double tropopause structures lead to difficulties in calculating diagnostics and in their interpretation. Figure 2 displays the location of the lower values of the thermal tropopause (green circles). We then choose the lowest levels of the thermal tropopause as reference level to calculate relative altitudes.

Figure 4 provides O<sub>3</sub> and CO profiles in relative altitude (RALT) coordinates for the four O<sub>3</sub>–CO correlations. Blue, red and green represent the stratospheric, tropospheric and transition CO and O<sub>3</sub> values, respectively, as selected in Sect. 3.1. Horizontal dashed lines provide the upper and lower estimated ExTL “boundaries” in RALT, corresponding to the 10 and 90 % deciles. More extreme percentile values, for example 2 and 98 %, could be chosen but would be influenced by extreme ExTL selected points, and might show strong variations in RALT space. Because the selection criteria are empirical and can allow for extreme RALT location ExTL points, we then decided to remove 10 % of each side of the distribution in order to have a reasonable indicator for the ExTL boundaries location. In the free-model

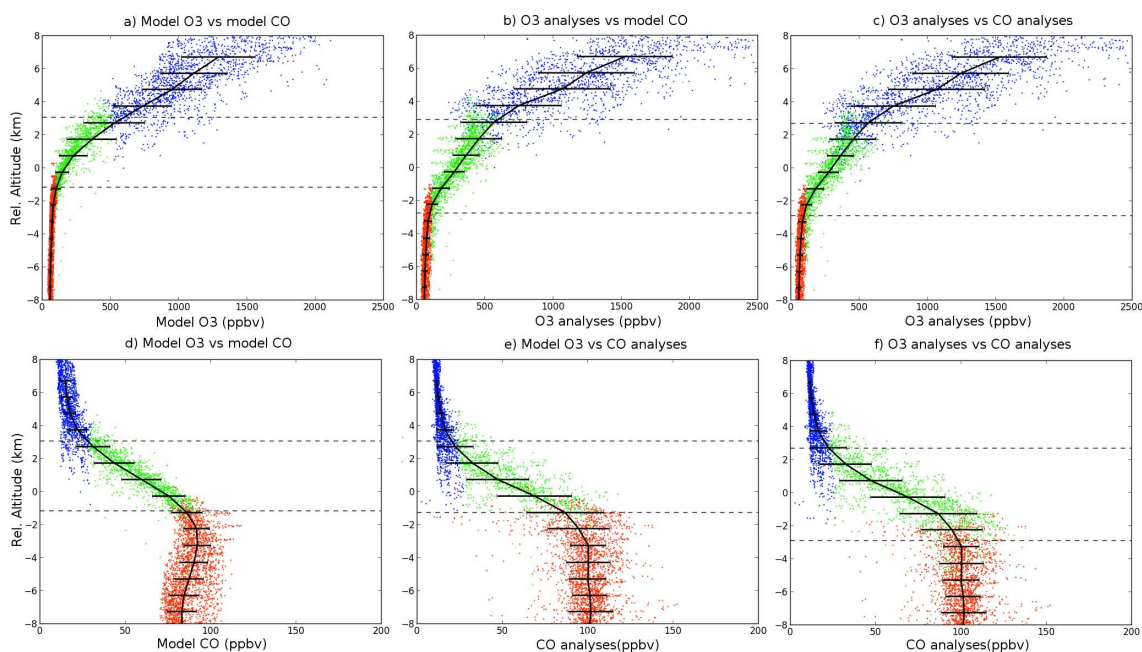


**Fig. 4.** O<sub>3</sub> and CO profiles in the region between 30° W–10° E and 40–65° N on 15 August 2007 at 12:00 UTC. O<sub>3</sub> profiles (ppbv) in altitude coordinates (km) relative to the 360 K level are provided for model O<sub>3</sub> vs. model CO (a), O<sub>3</sub> analyses vs. model CO (b) and O<sub>3</sub> analyses vs. CO analyses (c). CO profiles (ppbv) in relative altitude coordinates (km) are provided for model O<sub>3</sub> vs. model CO (d), model O<sub>3</sub> vs. CO analyses (e) and O<sub>3</sub> analyses vs. CO analyses (f). Following selection criteria, red and blue dots are identified as of tropospheric and stratospheric origin, respectively. The green dots are identified as the transitional layer between the stratosphere and the troposphere (see text for details). Black lines represent the mean profile every kilometer, and horizontal error bars show the 1σ standard deviation.

run simulations the upper and lower boundaries of the estimated ExTL are diagnosed at approximately 3 and –1 km, respectively (Fig. 4a and d). Positive and negative altitudes are below and above the thermal tropopause, respectively. Compared to the free-model run, O<sub>3</sub> analyses (Fig. 4b) show more O<sub>3</sub> in the ExTL (green dots) and in the troposphere (red dots). In relative altitude, the estimated ExTL extends into the troposphere to –3 km. The upper boundary height is not significantly modified but the lower boundary is lowered by 2 km. It has been shown that the tropospheric O<sub>3</sub> concentrations in MLS analyses (with MOCAGE) are increased due to downward transport during the STE event (Barré et al., 2012). Thus, some increased upper tropospheric O<sub>3</sub> values are greater than the tropospheric threshold defined in Sect. 3.1. In the CO profiles, analyses (Fig. 4e) show values greater than the values of the free run in the troposphere and lower than the values of the free run in the stratosphere. This leads to a stronger CO gradient in the ExTL around the thermal tropopause. This stronger gradient does not give a significantly narrower extent of the ExTL boundaries in RALT coordinates. The location of the estimated ExTL boundaries could differ significantly in the RALT space depending on O<sub>3</sub> analyses, and CO analyses are used separately or together. When O<sub>3</sub> analyses and CO analyses are used together in the diagnostics (Fig. 4c and f), the heights of the boundaries are close to those found on O<sub>3</sub> analyses and model CO. In the

next section, we further examine in detail the estimated ExTL distributions in the RALT space.

### 3.3 Diagnostic 3: sharpness of the transition

The third diagnostic provides the distribution of the estimated ExTL in relative altitude space (as defined in Sects. 3.1 and 3.2). The shape of the estimated ExTL distribution will allow for us to quantify its location and depth. Figure 5a–d displays the distributions for the various O<sub>3</sub>–CO relationships: model O<sub>3</sub> vs. model CO, O<sub>3</sub> analyses vs. model CO, model O<sub>3</sub> vs. CO analyses and O<sub>3</sub> analyses vs. CO analyses, respectively. Table 2 provides the heights of the mean and the standard deviation of the estimated ExTL distributions in relative altitude space. The free-model run distribution has its mean height at 1.42 km above the thermal tropopause with a standard deviation of 1.3 km. Studies using in situ aircraft measurement show that the ExTL is centered on the thermal tropopause with a narrower extent than observed in this study (Pan et al., 2004, 2007). In a multi-model assessment, Heggin et al. (2010) showed that models simulate an ExTL that is wider than observed in satellite observations, and shifted above the thermal tropopause. The low vertical resolution (800 m) in the model UTLS layers and also the low horizontal resolution (2° × 2°) used in this study is not sufficient to represent the sharp gradients of O<sub>3</sub> and CO observed at

**Table 2.** Heights of the mean, median and standard deviation of the ExTL distribution in relative altitude space (km) for the different experiments. Negative mean values and positive mean values are below and above the thermal tropopause, respectively.

	Mean	Standard Deviation
model O <sub>3</sub> vs. model CO	1.15	1.29
O <sub>3</sub> analyses vs. model CO	0.45	1.74
model O <sub>3</sub> vs. CO analyses	0.93	1.28
O <sub>3</sub> analyses vs. CO analyses	0.16	1.70

the tropopause. This results in a broad transition layer in the UTLS. Thus, in our case, a narrower and a lower altitude distribution would be considered as benefits from the data assimilation.

Compared to the model O<sub>3</sub> vs. model CO distribution, the O<sub>3</sub> analyses vs. model CO distribution shows an increased spread with a standard deviation of 2 km (Fig. 5b and Table 2) but a lower mean value of about 0.45 km. As described in Sect. 3.2, an increase of tropospheric O<sub>3</sub> values leads to a broadening of the estimated ExTL (down to RALT = -4 km) in the troposphere. No significant changes in the stratosphere (positive RALT values) of the distribution can be noted. The increase of O<sub>3</sub> in the upper troposphere leads to increase of the estimated ExTL depth toward negative RALT. Due to the low sensitivity of the stratospheric selection criterion to the O<sub>3</sub> variations, the stratospheric side of the estimated ExTL is not significantly modified. However, the STE is detected by the tropospheric selection criterion, and the distribution becomes skewed toward negative RALT coordinates. Pan et al. (2004) showed that skewed distributions, particularly toward negative relative altitudes, indicate active mixing from the stratosphere to the troposphere. Validation against independent measurements as in Barré et al. (2012) and LEA2010 shows that UTLS ozone fields are improved by MLS assimilation, and the overall effect of MLS assimilation is to increase the LMS ozone fields. Barré et al. (2012) also show that MLS assimilation increments in the lower stratosphere are transported into the troposphere during STE events. This impacts the troposphere by increasing its ozone mixing ratio. According to these previous studies, MLS analyses induce a more intense ozone mixing between the stratosphere and the troposphere. This ozone mass mixing should not to be confused with the air mass mixing, which is not changed in a CTM context. The skewed shape of the distribution then indicates this more intense ozone mixing from the stratosphere to the troposphere in MLS O<sub>3</sub> analyses than in the free-model run. Despite a wider spread of the estimated ExTL distribution, the O<sub>3</sub> analyses vs. model CO ExTL distribution shows a mean height closer to the thermal tropopause than the model O<sub>3</sub> vs. model CO ExTL distribution. This is consistent with Fig. 2c, where the height of ozone gradient in the O<sub>3</sub> analyses have a better match with the thermal tropopause height.

Compared to model O<sub>3</sub> vs. model CO distributions and the O<sub>3</sub> analyses vs. model CO distributions, the model O<sub>3</sub> vs. CO analyses provides a narrower estimated ExTL (Fig. 5c). The means of the distributions are reduced compared to model O<sub>3</sub> vs. model CO distribution, but not as much as for the O<sub>3</sub> analyses vs. model CO (see Table 2). The standard deviation is very slightly reduced (by 0.01 km). Compared to the free-model run, CO analyses increase CO concentrations in the upper troposphere around the STE. However, at the location of the intrusion, the reduced CO values in the upper troposphere are not detected by the tropospheric selection criterion (described in Sect. 3.1), which is not very sensitive to CO variations. Moreover, the stratospheric selection criterion is highly sensitive to CO variations. Compared to the model O<sub>3</sub> vs. model CO, the spread of the model O<sub>3</sub> vs. CO analyses distribution is reduced in the stratospheric side (positive RALT), whereas the tropospheric side (negative RALT) is not significantly modified. This lowers the mean value of the distribution.

The O<sub>3</sub> analyses vs. CO analyses distributions (Fig. 5d) have the same shape as the model O<sub>3</sub> vs. model CO distribution but are not narrowed. The mean of the distribution is very close to the thermal tropopause (0.16 km). The standard deviations are slightly lower than those of the O<sub>3</sub> analyses vs. model CO distributions but larger than those of the model O<sub>3</sub> vs. model CO distributions. The estimated ExTL distribution benefits from the combination of the information provided by O<sub>3</sub> analyses and CO analyses. CO analyses reduce the estimated ExTL distribution extent on its stratospheric side and O<sub>3</sub> analyses increase the estimated ExTL distribution extent on its tropospheric side.

Pan et al. (2004) found using aircraft measurements that the center of the ExTL is statistically associated with the thermal tropopause, and the thickness of this layer is ~2–3 km in the midlatitudes. In Table 2, the thickness of the estimated ExTL is ~3 km (2σ), and the mean and median values are lowered by ~1 km. Moreover, because of the rapid overturning of air masses in the troposphere and high static stability in the stratosphere, stratosphere-to-troposphere transport (STT) shows deeper signatures in altitude than troposphere-to-stratosphere transport (TST) (Hoor et al., 2002). Consequently, during STT events, the ExTL will show a skewed distribution toward negative RALT. This skewed distribution is only seen with O<sub>3</sub> analyses, which provide increased O<sub>3</sub> values in the LMS and below (see for example Fig. 2c) and allow for detection of the appropriate STT in these diagnoses.

Data assimilation of stratospheric O<sub>3</sub> limb measurements makes the following possible:

- i. It allows for the detection of deep stratospheric intrusion by providing better lower stratospheric ozone fields (see validation in LEA2010). The estimated ExTL distribution is skewed, extended and lowered as expected in a case of a stratospheric intrusion.

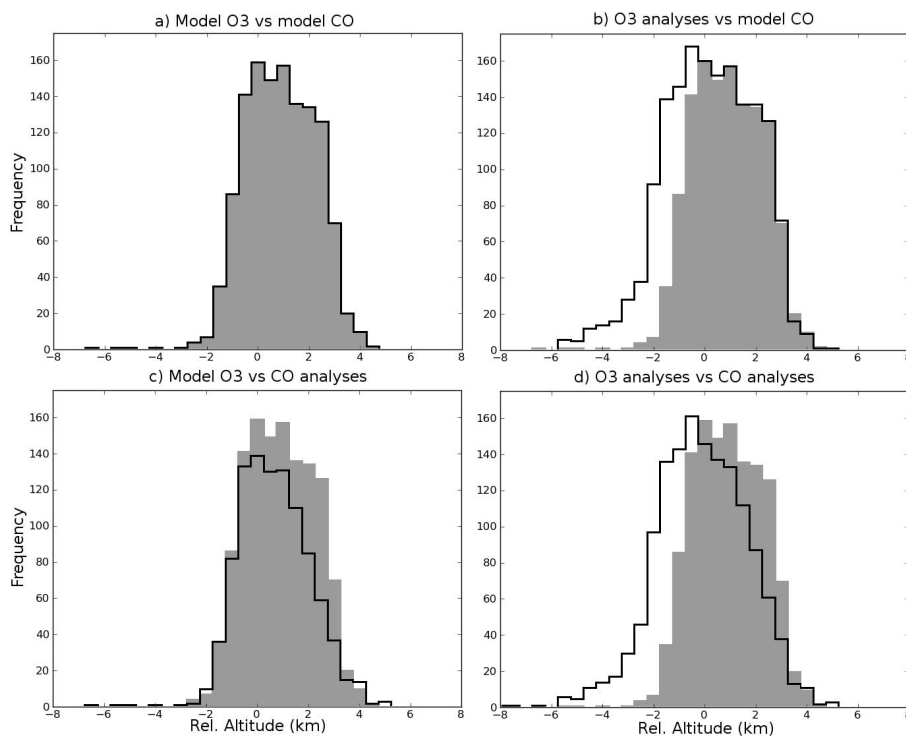


**Fig. 5.** Histograms showing the distributions of the ExTL in relative altitude space in the region between  $30^{\circ}$  W– $10^{\circ}$  E and  $40$ – $65^{\circ}$  N on 15 August 2007 at 12:00 UTC. model  $O_3$  vs. model CO (a),  $O_3$  analyses vs. model CO (b), model  $O_3$  vs. CO analyses (c) and  $O_3$  analyses vs. CO analyses (d) are displayed in black, and model  $O_3$  vs. model CO distribution is overplotted in gray on the plots. The histograms display the absolute frequencies.

- ii. It increases the ozone mixing ratio in the upper troposphere (Barré et al., 2012), resulting in an increase of the ExTL distribution spread.

Data assimilation of tropospheric CO nadir measurements has the following effects:

- i. It does not allow for detection of deep stratospheric signatures as efficiently as  $O_3$  limb measurements. The ExTL distribution is not significantly lowered and not skewed.
- ii. It improves the upper tropospheric CO fields (see validation in LEA2010), providing a sharper CO gradient in the UTLS and narrowing the ExTL distribution in its stratospheric side.

#### 4 Global ExTL for the month of August 2007

In this section, we apply the diagnostic of Sect. 3.3 (sharpness of the transition) on the global scale in order to investigate the impact of data assimilation of MOPITT CO and MLS  $O_3$  on the estimated ExTL. Because the STE activities near the extratropical tropopause are largely associated with synoptic scale dynamical processes that are on a timescale of a few days to a week, the variability in tracer fields induced

by these activities is largely smoothed out in the monthly mean fields. The diagnostics have been then performed on the 15 August 2007 12:00 UTC fields and on the monthly time-averaged (August 2007) fields. The diagnostics are applied on  $10^{\circ}$  S latitude bands and regression selection criteria take into account every latitude–longitude grid point in those latitude bands. We also only consider extratropical latitudes outside the  $20^{\circ}$  S– $20^{\circ}$  N range. Figure 6a–d show zonal means of the model  $O_3$ , model CO,  $O_3$  analyses and CO analyses for the month of August 2007 (i.e., longitude-time average), in tropopause–relative altitude coordinates. The lower white line is the 2 PVU level and the upper black line is the 380 K isentrope, denoting the LMS bounds. In general,  $O_3$  analyses increase the amount of  $O_3$  in the LMS, especially at northern extratropical latitudes poleward of  $50^{\circ}$  N (by more than 200 ppbv). CO analyses increase the tropospheric CO values, except between 20 and  $40^{\circ}$  N, and decrease the lower stratospheric CO values.

We estimate the distribution of the  $O_3$ –CO ExTL for latitude bands of  $10^{\circ}$  between  $90$  and  $20^{\circ}$  S and between  $20$  and  $90^{\circ}$  N with the same selection criteria as in Sect. 3.1. In Figs. 7 and 8, we provide the latitudinal variations of the estimated ExTL distribution for the 15 August 2007 and for the August average, respectively: median (red line), deciles (red- to pink-filled areas), mean (green line) and standard

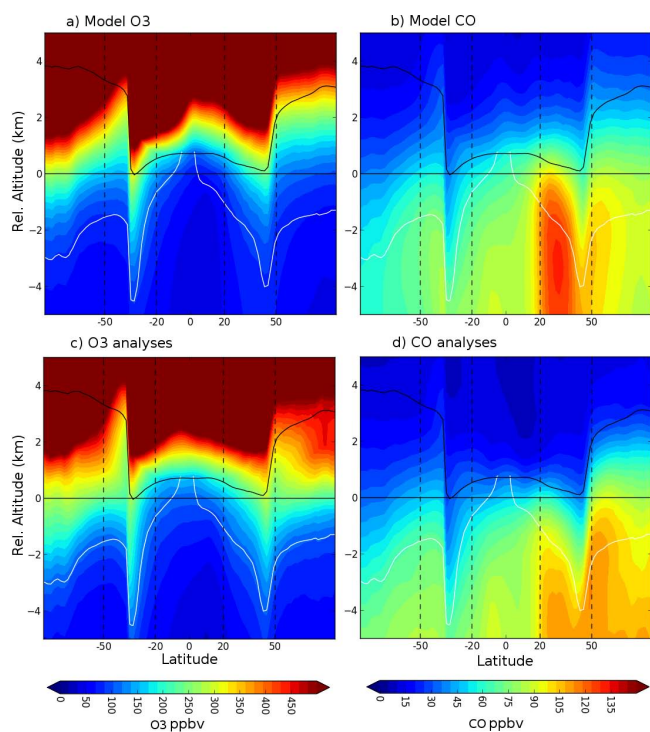


**Fig. 6.** Zonal averages for the month of August 2007 in relative altitudes (km) of model O<sub>3</sub> (a), model CO (b), O<sub>3</sub> analyses (c) and CO analyses (d). Dashed black vertical lines mark the regions of interest (i.e., 90–50° S, 50–20° S, 20–50° N and 50–90° N). The lowermost stratosphere bounds are represented by the 2PVU contour in absolute value (lower white line), and the 380 K isentropic contour (upper black line).

deviation from the mean (light green lines) in RALT coordinates. The LMS bounds (the lower blue line is the 2PVU level and the upper blue line is the 380 K isentropic) and the thermal tropopause (straight horizontal line) are also overplotted in RALT coordinates. The estimated ExTL distributions are provided for the four experiments: model O<sub>3</sub> vs. model CO, O<sub>3</sub> analyses vs. model CO, model O<sub>3</sub> vs. CO analyses and O<sub>3</sub> analyses vs. CO analyses. Tables 3 and 4 provide mean and standard deviation values for four regions – 90 to 50° S, 50 to 20° S, 20 to 50° N and 50 to 90° N – as defined by the dashed lines in the Figs. 7 and 8, respectively. The standard deviations are systematically higher in the distributions calculated from the 15 August 2007 (hereafter daily diagnostics) than in the distributions calculated from the monthly averaged (August 2007) fields (hereafter monthly diagnostics). As mentioned above, the variability associated with STE activities located at extratropical latitudes is smoothed out in the monthly means fields. This results in a narrower ExTL distribution estimate when a monthly mean field is used. However, the diagnostic on the monthly mean fields is useful to diagnose the behavior on the global estimated ExTL during the month of August 2007.

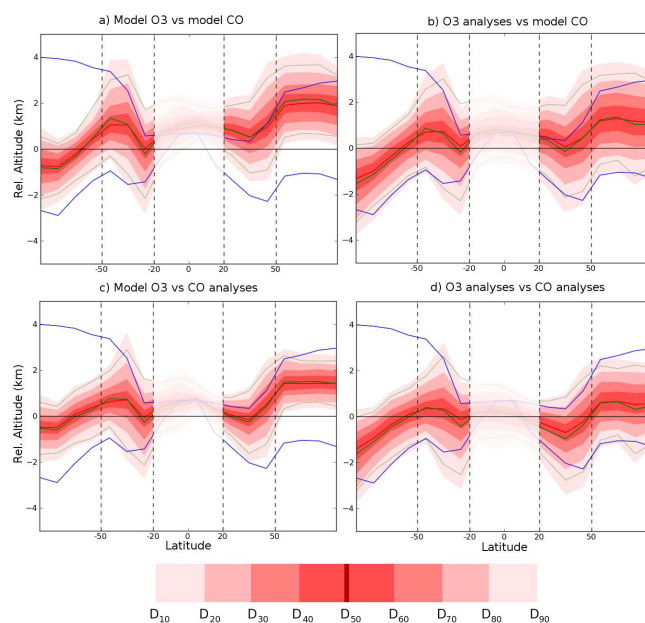


**Fig. 7.** Latitudinal height variations in altitude coordinates (km) relative to the 360 K level of the ExTL distribution for model O<sub>3</sub> vs. model CO (a), O<sub>3</sub> analyses vs. model CO (b), model O<sub>3</sub> vs. CO analyses (c) and O<sub>3</sub> analyses vs. CO analyses (d) calculated from the 15 August 2007 12:00 UTC tracer fields. Red-filled contours provide the decile altitudes of the distribution. Red and green lines are the median and mean altitudes, respectively. Blue lines show the lowermost stratosphere bounds: the lower line provides the 2PVU contour in absolute value, while the upper line provides the 380 K isentropic contour.

In the model O<sub>3</sub> vs. model CO distributions, the estimated ExTL has latitudinal variations in the RALT space (Figs. 7a and 8a). In the Southern Hemisphere, the estimated ExTL follows the 2PVU line (mean and median values), although 1.5 to 2 km above it. In the Southern Hemisphere the mean and median values of the estimated ExTL are located around the thermal tropopause. The estimated ExTL is located on negative RALT near the South Pole, positive RALT at the midlatitudes and RALT close to 0° at the subtropics. This variation of altitudes is more visible on distributions calculated with daily diagnostics than with monthly diagnostics for reasons mentioned above (the fields are smoothed). In the Northern Hemisphere the location of the estimated ExTL is found above the thermal tropopause by 1 to 2 km. Between 20 and 50° N the estimated ExTL is located at 0.8 and 0.6 km for daily and monthly diagnostics, respectively (Tables 3 and 4). Between 50° N and the North Pole the estimated ExTL is located at 2 and 1.9 km for daily and monthly diagnostics, respectively (Tables 3 and 4).

The standard deviation of the estimated ExTL distribution shows higher values in the Northern Hemisphere. In the Sect. 3 we have shown that the estimated ExTL distribution is wider at the location of STE events. In the case of a global

**Table 3.** Heights of the mean and standard deviation of the ExTL distribution in relative altitude space (km) for the different experiments and for the different latitude bands over the globe, calculated from 15 August 2007 12:00 UTC tracer fields. Negative and positive mean values are below and above the thermal tropopause, respectively.

		90–50° S	50–20° S	20–50° N	50–90° N
model O <sub>3</sub> vs. model CO	Mean	0.072	0.727	0.800	2.062
	Standard Deviation	1.195	1.913	1.555	1.467
O <sub>3</sub> analyses vs. model CO	Mean	−0.200	0.432	0.208	1.157
	Standard Deviation	1.342	2.060	1.962	1.969
model O <sub>3</sub> vs. CO analyses	Mean	0.106	0.403	0.036	1.466
	Standard Deviation	1.187	1.747	1.283	0.986
O <sub>3</sub> analyses vs. CO analyses	Mean	−0.240	0.076	−0.660	0.503
	Standard Deviation	1.290	1.941	1.714	1.648

**Table 4.** Heights of the mean and standard deviation of the ExTL distribution in relative altitude space (km) for the different experiments and for the different latitude bands over the globe, calculated from monthly average (August 2007) tracer fields. Negative and positive mean values are below and above the thermal tropopause, respectively.

		90–50° S	50–20° S	20–50° N	50–90° N
model O <sub>3</sub> vs. model CO	Mean	0.168	0.084	0.594	1.900
	Standard Deviation	0.940	1.418	1.323	1.331
O <sub>3</sub> analyses vs. model CO	Mean	−0.130	−0.090	0.048	1.248
	Standard Deviation	1.188	1.667	1.676	1.652
model O <sub>3</sub> vs. CO analyses	Mean	0.508	−0.080	−0.120	1.581
	Standard Deviation	0.666	1.131	1.006	0.876
O <sub>3</sub> analyses vs. CO analyses	Mean	0.152	−0.360	−0.700	0.713
	Standard Deviation	0.932	1.381	1.339	1.333

diagnostic, a wider extent of the estimated ExTL corresponds to a tendency of deeper exchanges between the stratosphere and the troposphere. The wider extent of the estimated ExTL in the Northern Hemisphere can be interpreted at the global scale as more intense STE activity. Two maxima of estimated ExTL thickness are also identified in both hemispheres near 35° S and 35° N, corresponding to the location of the subtropical jets where mixing processes occur (Gettelman et al., 2011). Pan et al. (2004) deduced from aircraft observations (in the Northern Hemisphere) of O<sub>3</sub> and CO an ExTL centered at the thermal tropopause with a thickness between 2 and 3 km expanding into a thicker layer in the vicinity of the subtropical jet.

The O<sub>3</sub> analyses vs. model CO data provides slightly wider distributions for the estimated ExTL for all latitudes (Figs. 7b and 8b) with a standard deviation that is increased by up to 0.5 km (between 50° N and the North Pole). When stratospheric O<sub>3</sub> profiles are assimilated, the model is unable to improve the strong O<sub>3</sub> gradients observed in the UTLS. These wider distributions also suggest a more intense O<sub>3</sub> mixing produced by MLS assimilation. As explained in Sect. 3.3, MLS assimilation increments that increase O<sub>3</sub>

in the LMS are advected through the tropopause and then increase the O<sub>3</sub> mixing. O<sub>3</sub> analyses move the estimated ExTL location to lower altitudes and always have median and mean values of the distribution below the 380 K level. The mean values of the distributions are significantly lowered in the Northern Hemisphere by −0.6 km in the subtropics and by −0.9 km in the middle and polar latitudes closer to the thermal tropopause. In the Southern Hemisphere the estimated ExTL mean location is not lowered as much (less than 0.1 km) than in the Northern Hemisphere. This can be explained by a significant increase of ozone in the LMS in the Northern Hemisphere but not in the Southern Hemisphere (Fig. 6c). Model O<sub>3</sub> vs. CO analyses (Figs. 7c and 8c) show reduction in the estimated ExTL thickness. The layer thickness is strongly reduced, as reflected in a reduction of the standard deviation by about −0.38 km in the Northern Hemisphere and by −0.18 km in the Southern Hemisphere. The mean and the median values match the thermal tropopause poleward of 50° S but remain 1.5 to 2 km above the thermal tropopause poleward of 50° N.

The distributions of O<sub>3</sub> analyses vs. CO analyses (Figs. 7d and 8d) combine the ExTL representation of the two

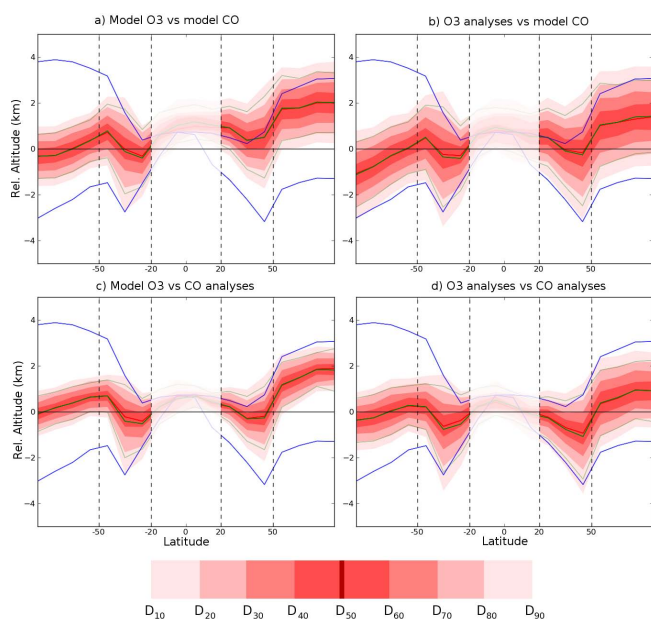


**Fig. 8.** Latitudinal height variations in altitude coordinates (km) relative to the 360 K level of the ExTL distribution for model O<sub>3</sub> vs. model CO (a), O<sub>3</sub> analyses vs. model CO (b), model O<sub>3</sub> vs. CO analyses (c) and O<sub>3</sub> analyses vs. CO analyses (d) calculated from the monthly mean tracer fields on August 2007. Red-filled contours provide the decile altitudes of the distribution. Red and green lines are the median and mean altitudes, respectively. Blue lines show the lowermost stratosphere bounds: the lower line provides the 2PVU contour in absolute value, the upper line provides the 380 K isentropic contour. Tropical latitudes are not shown.

previously described distributions (i.e., O<sub>3</sub> analyses vs. model CO distribution and model O<sub>3</sub> vs. CO analyses distribution). The standard deviations are not reduced, and show very similar values to those from model O<sub>3</sub> vs. model CO distributions (see Tables 3 and 4). In a general manner, the most significant changes in the estimated ExTL distributions are located in the Northern Hemisphere. The location of the estimated ExTL is lowered close to the thermal tropopause (due to O<sub>3</sub> analyses), and the spread of the distributions is conserved (due to CO analyses). No significant changes can be noted in the Southern Hemisphere, except near the South Pole in the daily distributions. In the subtropical latitudes, the estimated ExTL is located 1 km below the thermal tropopause. This region is subject to the thermal tropopause break at the location of the subtropical jet providing an instance of a double tropopause. It has been shown that the ExTL, at these latitudes, has a contribution from the subtropical jet, the tropical tropopause layer and the midlatitudes lowermost stratosphere, forming complex structures in the ExTL as double thermal tropopause features (Vogel et al., 2011). In this study, only the lower thermal tropopause altitudes have been taken in account to perform the diagnostics. At subtropical latitudes, the ExTL distribution could

be more centered on the higher thermal tropopause occurrence, where strong tropospheric-to-stratospheric intrusions from the tropical tropopause layer are existent. This could impact the diagnostics providing shifted ExTL distribution on positive RALT.

In this section, we have shown the impacts of data assimilation on the the ExTL representation between the stratosphere and the troposphere at a global scale in the extratropics. Due to the shape of the O<sub>3</sub>–CO relationship and the selection criteria described in Sect. 3.1, the upper bound of the ExTL distribution is mostly sensitive to CO variations, whereas the lower bound of the ExTL distribution is mostly sensitive to O<sub>3</sub> variations. CO analyses have more influence on the stratospheric side of the estimated ExTL and reduce the mixing layer depth. O<sub>3</sub> analyses have more influence on the tropospheric side of the estimated ExTL and are not able to reduce the estimated ExTL depth but have the capability to represent deeper STE signatures at extratropical latitudes. This lowers the location of the estimated ExTL closer to the thermal tropopause. A combination of these two analyses shows significantly better results than each analysis separately: the estimated ExTL location matches the thermal tropopause location at middle and polar latitudes, and its spread is in the range of what is observed by in situ and satellite measurements studies. In the Northern Hemisphere, Pan et al. (2004) deduced from aircraft observations that the ExTL thickness is 2–3 km at midlatitudes, with enhanced values in the vicinity of the subtropical jet. In Tables 3 and 4, the O<sub>3</sub> analyses vs. CO analyses distribution shows a standard deviation ( $2\sigma$ ) in a range from  $\sim 2.7$  to  $\sim 3.4$  km between 50 and 90° N. Hegglin et al. (2009) found in satellite measurements an ExTL depth in extratropical latitudes between 1.5 and 4 km that matches our results.

## 5 Discussions and conclusions

In this study, we use the statistical diagnostics defined by Pan et al. (2004) and Pan et al. (2007) to provide a quantitative description of the impact of MLS O<sub>3</sub> and MOPITT CO analyses produced by data assimilation on the ExTL. Firstly, we focus on a STE case study documented and validated by El Amraoui et al. (2010). O<sub>3</sub>–CO relationships are used to estimate the height and depth of the ExTL. Two different O<sub>3</sub> fields are provided, a MOCAGE free-model run and MLS analyses; and two different CO fields are provided, a MOCAGE free-model run and MOPITT analyses. Then four O<sub>3</sub>–CO relationships are studied. Diagnosing assimilated fields with tracer–tracer correlations allows for us to evaluate the consistency between the different fields (assimilated or not). A direct conclusion of this study is the following: it is necessary to have assimilated each tracer field that is diagnosed to keep a relative consistency. The following question is left open: does assimilation of exactly collocated measurements

of different tracers (e.g., from the same atmospheric sounder) provide a better consistency in the tracer–tracer relationship?

In addition to diagnosing the effect of data assimilation on the O<sub>3</sub>–CO relationship, we also diagnose the ExTL estimated distribution in the relative altitude space. The free-model run O<sub>3</sub>–CO relationship shows a 2.5 km wide ExTL distribution that is centered 1 km above the thermal tropopause. This distribution shows the typical behavior of the models representing the atmospheric composition, namely an overestimation of the ExTL depth and of its location in height, above the thermal tropopause. MLS O<sub>3</sub> analyses extend the spread of the distribution toward tropospheric altitudes due to an increase of O<sub>3</sub> values in the UTLS. This increases the depth of the ExTL by about 1 km and lowers the mean location by 0.7 km closer to the thermal tropopause. The estimated ExTL distribution is skewed toward tropopause-relative altitudes, showing the capability of MLS O<sub>3</sub> analyses to accentuate the ozone signature of the STE event. MOPITT CO analyses have the capability to sharpen the CO gradient in the UTLS. This slightly reduces the spread of the ExTL on its stratospheric side, showing a mean location closer to the thermal tropopause. Due to the low sensitivity to CO tropospheric variations of the diagnostics used in the present study, MOPITT CO analyses do not show a signature of STE in the estimated ExTL distributions. In combining the information provided by MLS O<sub>3</sub> analyses and MOPITT CO analyses, the estimated ExTL distribution has a more realistic shape and location. The ExTL mean location is centered on the thermal tropopause, but the spread of the ExTL is increased compared to the free-model run. It has been shown that models simulate an ExTL deeper than observed in aircraft measurements, and shifted above the thermal tropopause (Hegglin et al., 2010). This is due to the limited vertical and horizontal resolutions of the models, as well as the lack of representativeness in the aircraft observations. However, data assimilation of CO and O<sub>3</sub> satellite measurements helps to improve the representation of the ExTL, and tries to overcome the limitation due to the relatively low model resolution.

We also extend the diagnostics at global extratropical latitudes for the August 2007 time period. MLS O<sub>3</sub> analyses show a spread of the estimated ExTL distribution toward the surface, which lowers its mean location closer to the thermal tropopause. MOPITT CO analyses reduce the spread of the estimated ExTL on its stratospheric side, which also lowers its mean location closer to the thermal tropopause. When MLS O<sub>3</sub> analyses and MOPITT CO analyses are used together, a synergistic effect is observed. The ExTL location poleward of 50° N and 50° S matches the thermal tropopause, and the depth of the estimated ExTL is conserved compared to the free-model run O<sub>3</sub>–CO diagnostics. As shown in the case study, the STE is characterized by the tropospheric extent of the ExTL. In the global diagnostics, MLS O<sub>3</sub> analyses increase the tropospheric extent of the ExTL distribution below the 2 PVU level, showing a more intense O<sub>3</sub> mixing from

stratosphere to troposphere. Further investigation is needed, for example using O<sub>3</sub> and CO fields analyses over longer timescales (e.g., more than 1 yr) to diagnose the seasonal behavior of the ExTL.

*Acknowledgements.* We thank the reviewers for their constructive comments that helped to improve the article. We thank the Jet Propulsion Laboratory MLS science team for retrieving and providing the O<sub>3</sub> MLS data. We thank the National Center for Atmospheric Research MOPITT science team and NASA for producing and archiving the MOPITT CO product. This work was funded by the Centre National de Recherches Scientifiques (CNRS) and the Centre National de Recherches Météorologiques (CNRM) of Météo-France. V.-H. Peuch, J.-L. Attié, L. El Amraoui and W. A. Lahoz are supported by the RTRA/STAE (POGEQA project). J.-L. Attié thanks also the Région Midi Pyrénées (INFOAIR project).

Edited by: M. Palm



The publication of this article is financed by CNRS-INSU.

## References

- Barré, J., Peuch, V.-H., Attié, J.-L., El Amraoui, L., Lahoz, W. A., Josse, B., Claeyman, M., and Nédélec, P.: Stratosphere-troposphere ozone exchange from high resolution MLS ozone analyses, *Atmos. Chem. Phys.*, 12, 6129–6144, doi:10.5194/acp-12-6129-2012, 2012.
- Barret, B., Ricaud, P., Mari, C., Attié, J.-L., Bousserez, N., Josse, B., Le Flochmoën, E., Livesey, N. J., Massart, S., Peuch, V.-H., Piacentini, A., Sauvage, B., Thouret, V., and Cammas, J.-P.: Transport pathways of CO in the African upper troposphere during the monsoon season: a study based upon the assimilation of spaceborne observations, *Atmos. Chem. Phys.*, 8, 3231–3246, doi:10.5194/acp-8-3231-2008, 2008.
- Bechtold, P., Bazile, E., Guichard, F., Mascart, P., and Richard, E.: A mass-flux convection scheme for regional and global models, *Q. J. Roy. Meteor. Soc.*, 96, 869–886, 2001.
- Bencherif, H., Amraoui, L. E., Sernane, N., Massart, S., Charyulu, D. V., Hauchecorne, A., and Peuch, V.-H.: Examination of the 2002 major warming in the southern hemisphere using ground-based and Odin/SMR assimilated data: stratospheric ozone distributions and tropic/mid-latitude exchange, *Can. J. Phys.*, 85, 1287–1300, 2007.
- Buis, S., Piacentini, A., and Déclat, D.: PALM: a computational framework for assembling high-performance computing applications, *Concurrency Computat.: Pract. Exper.*, 18, 231–245, doi:10.1002/cpe.914, 2006.
- Cathala, M. L., Pailleux, J., and Peuch, V.-H.: Improving chemical simulations of the upper troposphere–lower stratosphere with sequential assimilation of MOZAIC data, *Tellus B*, 55, 1–10, 2003.

- Courtier, P., Freydisier, C., Geleyn, J. F., Rabier, F., and Rochas, M.: The ARPEGE project at Météo France, in: *Atmospheric Models*, 2, 193–231, Workshop on Numerical Methods, Reading, UK, 1991.
- Drummond, J. R. and Mand, G. S.: Evaluation of operational radiances for the Measurement of Pollution in the Troposphere (MOPITT) instrument CO thermal-band channels, *J. Geophys. Res.*, 109, D03308, doi:10.1029/2003JD003970, 1996.
- Dufour, A., Amodei, M., Ancellet, G., and Peuch, V.-H.: Observed and modelled "chemical weather" during ESCOMPTE, *Atmos. Res.*, 74, 161–189, doi:10.1016/j.atmosres.2004.04.013, 2005.
- El Amraoui, L., Peuch, V.-H., Ricaud, P., Massart, S., Semane, N., Teyssède, H., Cariolle, D., and Karcher, F.: Ozone loss in the 2002–2003 Arctic vortex deduced from the assimilation of Odin/SMR O<sub>3</sub> and N<sub>2</sub>O measurements: N<sub>2</sub>O as a dynamical tracer, *Q. J. Roy. Meteor. Soc.*, 134, 217–228, doi:10.1002/qj.191, 2008a.
- El Amraoui, L., Semane, N., Peuch, V.-H., and Santee, M. L.: Investigation of dynamical processes in the polar stratospheric vortex during the unusually cold winter 2004/2005, *Geophys. Res. Lett.*, 35, L03803, doi:10.1029/2007GL031251, 2008b.
- El Amraoui, L., Attié, J.-L., Semane, N., Claeysman, M., Peuch, V.-H., Warner, J., Ricaud, P., Cammas, J.-P., Piacentini, A., Josse, B., Cariolle, D., Massart, S., and Bencherif, H.: Midlatitude stratosphere – troposphere exchange as diagnosed by MLS O<sub>3</sub> and MOPITT CO assimilated fields, *Atmos. Chem. Phys.*, 10, 2175–2194, doi:10.5194/acp-10-2175-2010, 2010.
- Fischer, H., Wienhold, F. G., Hoor, P., Bujok, O., Schiller, C., Siegmund, P., Ambaum, M., Scheeren, H. A., and Lelieveld, J.: Tracer correlations in the northern high latitude lowermost stratosphere: Influence of cross-tropopause mass exchange, *Geophys. Res. Lett.*, 27, 97–100, doi:10.1029/1999GL010879, 2000.
- Fisher, M. and Andersson, E.: Developments in 4D-Var and Kalman filtering, in: *Technical Memorandum Research Department*, vol. 347, ECMWF, Reading, UK, 2001.
- Geer, A. J., Lahoz, W. A., Bekki, S., Bormann, N., Errera, Q., Eskes, H. J., Fonteyn, D., Jackson, D. R., Juckes, M. N., Massart, S., Peuch, V.-H., Rharmili, S., and Segers, A.: The ASSET intercomparison of ozone analyses: method and first results, *Atmos. Chem. Phys.*, 6, 5445–5474, doi:10.5194/acp-6-5445-2006, 2006.
- Gottelman, A., Hoor, P., Pan, L. L., Randel, W. J., Hegglin, M. I., and Birner, T.: The Extratropical Upper Troposphere and Lower Stratosphere, *Rev. Geophys.*, 49, RG3003, doi:10.1029/2011RG000355, 2011.
- Hegglin, M. I., Boone, C. D., Manney, G. L., and Walker, K. A.: A global view of the extratropical tropopause transition layer from Atmospheric Chemistry Experiment Fourier Transform Spectrometer O<sub>3</sub>, H<sub>2</sub>O, and CO, *J. Geophys. Res.*, 114, D00B11, doi:10.1029/2008JD009984, 2009.
- Hegglin, M. I., Gottelman, A., Hoor, P., Krichevsky, R., Manney, G. L., Pan, L. L., Son, S. W., Stiller, G., Tilmes, S., Walker, K. A., Eyring, V., Shepherd, T. G., Waugh, D., Akiyoshi, H., Anel, J. A., Austin, J., Baumgaertner, A., Bekki, S., Braesicke, P., Bruehl, C., Butchart, N., Chipperfield, M., Dameris, M., Dhomse, S., Frith, S., Garny, H., Hardiman, S. C., Joeckel, P., Kinnison, D. E., Lamarque, J. F., Mancini, E., Michou, M., Morgenstern, O., Nakamura, T., Olivie, D., Pawson, S., Pitari, G., Plummer, D. A., Pyle, J. A., Rozanov, E., Scinocca, J. F., Shibata, K., Smale, D., Teyssède, H., Tian, W., and Yamashita, Y.: Multimodel assessment of the upper troposphere and lower stratosphere: Extratropics, *J. Geophys. Res.*, 115, D00M09, doi:10.1029/2010JD013884, 2010.
- Holton, J. R., Haynes, P. H., McIntyre, M. E., Douglass, A. R., Rood, R. B., and Pfister, L.: Stratosphere-troposphere exchange, *Rev. Geophys.*, 4, 403–439, 1995.
- Homeyer, C. R., Bowman, K. P., and Pan, L. L.: Extratropical tropopause transition layer characteristics from high-resolution sounding data, *J. Geophys. Res.*, 115, D13108, doi:10.1029/2009JD013664, 2010.
- Hoor, P., Fischer, H., Lange, L., Lelieveld, J., and Brunner, D.: Seasonal variations of a mixing layer in the lowermost stratosphere as identified by the CO-O<sub>3</sub> correlation from in situ measurements, *J. Geophys. Res.*, 107, doi:10.1029/2000JD000289, 2002.
- Hoor, P., Gurk, C., Brunner, D., Hegglin, M. I., Wernli, H., and Fischer, H.: Seasonality and extent of extratropical TST derived from in-situ CO measurements during SPURT, *Atmos. Chem. Phys.*, 4, 1427–1442, doi:10.5194/acp-4-1427-2004, 2004.
- Jackson, D. R.: Assimilation of EOS MLS ozone observations in the Met Office data-assimilation system, *Q. J. Roy. Meteor. Soc.*, 133, 1771–1788, doi:10.1002/qj.140, 2007.
- Josse, B., Simon, P., and Peuch, V.-H.: Radon global simulation with the multiscale chemistry transport model MOCAGE, *Tellus*, 56, 339–356, 2004.
- Kalnay, E.: *Atmospheric modeling, data assimilation, and predictability*, University Press, Cambridge, 2003.
- Lahoz, W. A., Errera, Q., Swinbank, R., and Fonteyn, D.: Data assimilation of stratospheric constituents: a review, *Atmos. Chem. Phys.*, 7, 5745–5773, doi:10.5194/acp-7-5745-2007, 2007.
- Lefèvre, F., Brasseur, G. P., Folkens, I., Smith, A. K., and Simon, P.: Chemistry of the 1991–1992 stratospheric winter: three dimensional model simulations, *J. Geophys. Res.*, 99, 8183–8195, 1994.
- Louis, J.-F.: Parametric model of vertical eddy fluxes in the atmosphere, *Bound.-Lay. Meteorol.*, 17, 187–202, 1979.
- Massart, S., Cariolle, D., and Peuch, V.-H.: Towards an improvement of the atmospheric ozone distribution and variability by assimilation of satellite data, *C. R. Geosci.*, 337, 1305–1310, doi:10.1016/j.crte.2005.08.001, 2005.
- Massart, S., Piacentini, A., Cariolle, D., El Amraoui, L., and Semane, N.: Assessment of the quality of the ozone measurements from the Odin/SMR instrument using data assimilation, *Can. J. Phys.*, 85, 1209–1223, 2007.
- Pan, L. L., Randel, W. J., Gary, B. L., Mahoney, M. J., and Hints, E. J.: Definitions and sharpness of the extratropical tropopause: A trace gas perspective, *J. Geophys. Res.*, 109, D23103, doi:10.1029/2004JD004982, 2004.
- Pan, L. L., Wei, J. C., Kinnison, D. E., Garcia, R. R., Wuebbles, D. J., and Brasseur, G. P.: A set of diagnostics for evaluating chemistry-climate models in the extratropical tropopause region, *J. Geophys. Res.*, 112, D09316, doi:10.1029/2006JD007792, 2007.
- Pan, L. L., Randel, W. J., Gille, J. C., Hall, W. D., Nardi, B., Massie, S., Yudin, V., Khosravi, R., Konopka, P., and Tarasick, D.: Tropospheric intrusions associated with the secondary tropopause, *J. Geophys. Res.*, 114, D10302, doi:10.1029/2008JD011374, 2009.
- Peuch V.-H., Amodei, M., Barthet, T., Cathala, M.-L., Josse, B., Michou, M., and Simon, P.: MOCAGE, MOdèle de Chimie Atmo-

- sphérique à Grande Echelle, Proceedings of Météo-France workshop on atmospheric modelling, december 1999, 33-36, 1999.
- Plumb, R. A.: Tracer interrelationships in the stratosphere, *Rev. Geophys.*, 45, RG4005, doi:10.1029/2005RG000179, 2007.
- Ricaud, P., Barret, B., Attié, J.-L., Motte, E., Le Flochmoën, E., Teysseïdre, H., Peuch, V.-H., Livesey, N., Lambert, A., and Pommereau, J.-P.: Impact of land convection on troposphere-stratosphere exchange in the tropics, *Atmos. Chem. Phys.*, 7, 5639–5657, doi:10.5194/acp-7-5639-2007, 2007.
- Semane, N., Peuch, V.-H., Amraoui, L. E., Bencherif, H., Massart, S., Cariolle, D., Attié, J.-L., and Abidab, R.: An observed and analysed stratospheric ozone intrusion over the high Canadian Arctic UTLS region during the summer of 2003, *Q. J. Roy. Meteor. Soc.*, 133, 171–178, doi:10.1002/qj.141, 2007.
- Stajner, I., Wargan, K., Pawson, S., Hayashi, H., Chang, L.-P., Hudman, R. C., Froidevaux, L., Livesey, N., Levelt, P. F., Thompson, A. M., Tarasick, D. W., Stuebi, R., Andersen, S. B., Yela, M., Koenig-Langlo, G., Schmidlin, F. J., and Witte, J. C.: Assimilated ozone from EOS-Aura: Evaluation of the tropopause region and tropospheric columns, *J. Geophys. Res.*, 113, D16S32, doi:10.1029/2007JD008863, 2008.
- Stockwell, W. R., Kirchner, F., Khun, M., and Seefeld, S.: A new mechanism for regional atmospheric chemistry modelling, *J. Geophys. Res.*, 102, 25847–25879, 1997.
- Vogel, B., Pan, L. L., Konopka, P., Guenther, G., Mueller, R., Hall, W., Campos, T., Pollack, I., Weinheimer, A., Wei, J., Atlas, E. L., and Bowman, K. P.: Transport pathways and signatures of mixing in the extratropical tropopause region derived from Lagrangian model simulations, *J. Geophys. Res.*, 116, D05306, doi:10.1029/2010JD014876, 2011.
- Wargan, K., Pawson, S., Stajner, I., and Thouret, V.: Spatial structure of assimilated ozone in the upper troposphere and lower stratosphere, *J. Geophys. Res.*, 115, D24316, doi:10.1029/2010JD013941, 2010.
- Waters, J. W., Froidevaux, L., Harwood, R. S., Jarnot, R. F., Pickett, H. M., Read, W. G., Siegel, P. H., Cofield, R. E., Filipiak, M. J., Flower, D. A., Holden, J. R., Lau, G. K. K., Livesey, N. J., Manney, G. L., Pumphrey, H. C., Santee, M. L., Wu, D. L., Cuddy, D. T., Lay, R. R., Loo, M. S., Perun, V. S., Schwartz, M. J., Stek, P. C., Thurstans, R. P., Boyles, M. A., Chandra, K. M., Chavez, M. C., Chen, G. S., Chudasama, B. V., Dodge, R., Fuller, R. A., Girard, M. A., Jiang, J. H., Jiang, Y. B., Knosp, B. W., LaBelle, R. C., Lam, J. C., Lee, K. A., Miller, D., Oswald, J. E., Patel, N. C., Pukala, D. M., Quintero, O., Scaff, D. M., Snyder, W. V., Tope, M. C., Wagner, P. A., and Walch, M. J.: The Earth Observing System Microwave Limb Sounder (EOS MLS) on the Aura satellite, *IEEE T. Geosci. Remote*, 44, 1075–7092, 2006.
- World Meteorological Organization: Scientific Assessment of Ozone Depletion: 2002, Global ozone research and monitoring project report no. 47, 2003.
- Zahn, A., Brenninkmeijer, C. A. M., Maiss, M., Scharffe, D. H., Crutzen, P. J., Hermann, M., Heintzenberg, J., Wiedensohler, A., Gusten, H., Heinrich, G., Fischer, H., Cuijpers, J. W. M., and van Velthoven, P. F. J.: Identification of extratropical two-way troposphere-stratosphere mixing based on CARIBIC measurements of O<sub>3</sub>, CO, and ultrafine particles, *J. Geophys. Res.*, 105, 1527–1535, doi:10.1029/1999JD900759, 2000.